Near-ideal electrical properties of InAs/WSe_2 van der Waals heterojunction diodes

Cite as: Appl. Phys. Lett. **102**, 242101 (2013); https://doi.org/10.1063/1.4809815
Submitted: 25 March 2013 . Accepted: 09 April 2013 . Published Online: 17 June 2013

Steven Chuang, Rehan Kapadia, Hui Fang, Ting Chia Chang, Wen-Chun Yen, Yu-Lun Chueh, and Ali Javey

Near-ideal electrical properties of InAs/WSe_2 van der Waals heterojunction diodes

Steven Chuang,[1,2] Rehan Kapadia,[1,2] Hui Fang,[1,2,3] Ting Chia Chang,[1] Wen-Chun Yen,[4] Yu-Lun Chueh,[4] and Ali Javey[1,2,3,a)]
[1]*Electrical Engineering and Computer Sciences, University of California, Berkeley, California 94720, USA*
[2]*Berkeley Sensor and Actuator Center, University of California, Berkeley, California 94720, USA*
[3]*Materials Sciences Division, Lawrence Berkeley National Laboratory, Berkeley, California 94720, USA*
[4]*Materials Science and Engineering, National Tsing Hua University, Hsinchu 30013, Taiwan*

(Received 25 March 2013; accepted 9 April 2013; published online 17 June 2013)

Here, we present the fabrication and electrical analysis of InAs/WSe_2 van der Waals heterojunction diodes formed by the transfer of ultrathin membranes of one material upon another. Notably, InAs and WSe_2 are two materials with completely different crystal structures, which heterojunction is inconceivable with traditional epitaxial growth techniques. Clear rectification from the *n*-InAs/*p*-WSe_2 junction (forward/reverse current ratio $>10^6$) is observed. A low reverse bias current $<10^{-12}$A/μm^2 and ideality factor of $\sim$1.1 were achieved, suggesting near-ideal electrically active interfaces. © *2013 AIP Publishing LLC*. [http://dx.doi.org/10.1063/1.4809815]

The development of heterojunctions has led to numerous high impact discoveries and applications.[1–5] Heterostructures are typically grown with epitaxial methods to ensure the high quality and crystallinity of the participating material layers. However in order to obtain high quality interfaces with traditional epitaxial methods, the lattice constant and crystal structure of each participating material must be similar. This severely limits the possible material pairs that could be utilized in heterostructures. Many research efforts have focused on resolving this issue.[6–14] One path to overcome this limitation would be to form a heterostructure by layer transfer of its components. The key advantage of this method is that it would theoretically allow for the complete freedom of material choice in the hetero-stacks. In addition, there would be no interdiffusion of atoms at the interface, given that the transfer is conducted at room temperature. It remains unclear whether high quality interfaces without large density of trap states and with near-ideal electrical characteristics can be obtained with this method. So far, van der Waals heterojunctions have not been thoroughly explored for materials other than carbon nanotubes, graphene, boron nitride, and tungsten disulphide.[10–14] Here, we fabricate InAs/WSe_2 thin film diodes by transferring their respective quantum membranes (QMs) upon one another. Notably, this heterostructure consists of two materials with completely different crystal structures (Figure 1(b)). An ideality factor of $\sim$1.1 and low reverse bias currents were measured, suggesting a clean interface between the two materials. Simulations were used to investigate the band structure and I-V characteristics of the diode.

The InAs/WSe_2 system was chosen to demonstrate the viability of this layer transfer heterostructure method since previously we have shown layer transferred InAs and WSe_2 membranes exhibiting low density of interface traps. The transfer of ultra-thin, high quality single crystalline InAs QMs has been thoroughly explored.[15–23] High performance WSe_2 devices have been demonstrated with the mechanical exfoliation technique.[24] In particular, WSe_2 is an ideal bottom layer for the heterostructure because it provides a freshly cleaved, pristine top surface, as demonstrated by the 60 mV/decade subthreshold slope exhibited by its MOSFETs.[24] Given that InAs and WSe_2 layers are intrinsically n-type and p-type, respectively, their combined structure will form a diode for electrical analysis of the interface. It is particularly important to reduce the Schottky barriers to each semiconductor, as Schottky diodes might mask the pn-junction diode performance. Low resistance metal contacts are readily formed to InAs as previously reported due to its low conduction band edge.[25] On the other hand, it is hard to form ohmic metal contacts with WSe_2 due to its large bandgap. Previous studies by our group have shown that the Schottky barrier to WSe_2 can be significantly thinned by NO_2 doping,[24] thereby enabling formation of low resistance contacts for hole injection.

The fabrication process of the InAs/WSe_2 van der Waals stack is as follows. WSe_2 QMs were first mechanically exfoliated onto a Si/SiO_2 (270 nm) substrate as previously described.[24] InAs QMs were then transferred from an epitaxial substrate onto the WSe_2 QMs.[15] The InAs QMs were dipped in 1%HF for $\sim$1 min to clean its surface right before being transferred onto the WSe_2 QMs. Pd contacts ($\sim$40 nm thick) were defined on the InAs and WSe_2 QMs by electron beam lithography, metallization, and lift-off. The Si substrate is heavily doped and serves as the global back gate. Figure 1(a) shows a cross-sectional diagram of the fabricated devices.

Figure 1(c) shows a transmission electron microscopy (TEM) image of an InAs/WSe_2 stack. From the TEM image, we see a distinct InAs single-crystal membrane stacked on a layered WSe_2 crystal with a $\sim$2.4 nm thick intermediate layer in-between. Previous InAs QM studies suggest that the intermediate layer is the native oxide of InAs.[15] WSe_2 is a 2D crystal that perfectly terminates on its surface and does not form native oxides under ambient conditions. The InAs/WSe_2 stack appears conformal, with no voids formed between the layers at least within the area examined by TEM. Through device simulations later in this paper, we

a)Electronic mail: ajavey@berkeley.edu

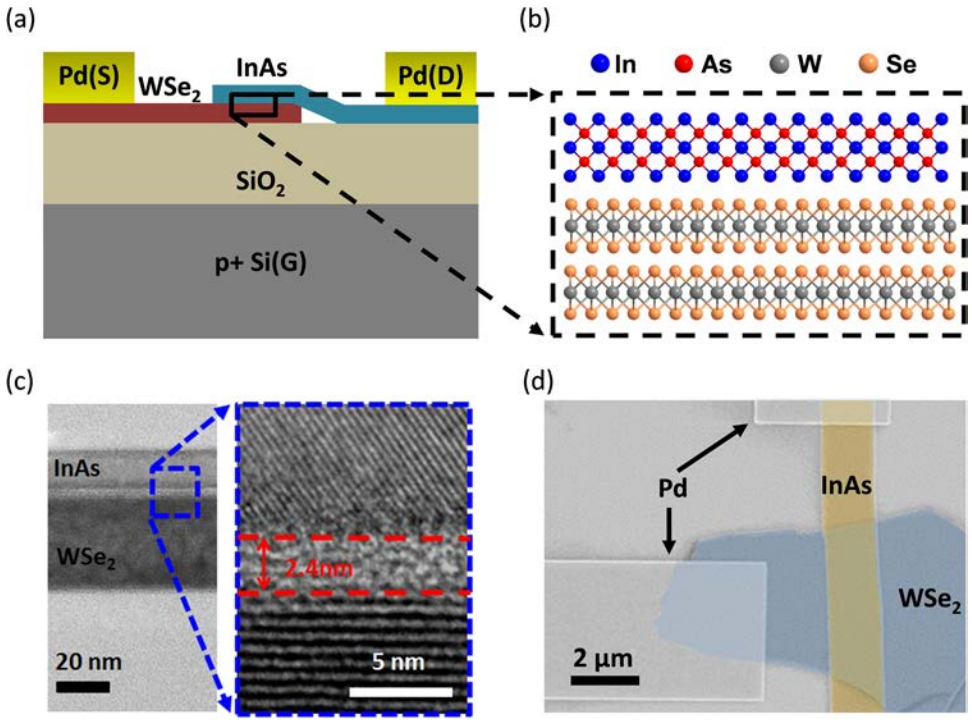

FIG. 1. (a) Cross-sectional schematic of an InAs/WSe_2 device explored in this study. (b) Ideal atomic cross-sectional view of InAs/WSe_2 interface, depicting 2 different crystal structures. (c) HRTEM image of fabricated InAs/WSe_2 heterostructure. (d) False color SEM image of fabricated InAs/WSe_2 device.

demonstrate that this system can be treated as though the InAs was stacked directly on top of WSe_2, and the effect of the ultra-thin intermediate oxide on the diode characteristics is negligible.

Scanning electron microscopy (SEM) image of an InAs/WSe_2 diode is depicted in Figure 1(d) and electrical characterization of a representative device (junction area $\sim 2.5\ \mu m^2$) is shown in Figure 2. Without any post-fabrication treatment (i.e., no surface doping of WSe_2), the device exhibits clear rectifying behavior (Fig. 2(a)). The reverse bias current was below the noise floor of the measurement. The relatively low forward bias current can be ascribed to the large contact resistance from the WSe_2/Pd junction. By grounding the WSe_2 electrode and increasing V_{SG}, we observe an increase in forward bias current caused by the modulation of the WSe_2/Pd Schottky junction contact resistance (Fig. 2(a)). The lack of gate dependence of the ideal diode region suggests that V_{SG} has a negligible effect on the InAs/WSe_2 junction and its band alignments. An ideality factor of ~ 1.1 is obtained, indicating a clean interface between the InAs and WSe_2 QMs. In order to reduce the WSe_2/Pd contact resistance, we exposed the devices to NO_2 gas (Fig. 2(b)). As previously reported, NO_2 molecules cause strong *p*-doping of WSe_2 and result in near ohmic Pd contacts to the valence band of WSe_2. On the other hand, NO_2 treatment does not affect the InAs conductivity and InAs/Pd junction. Previous studies have shown that InAs conduction changes $<2\times$ under exposure to NO_2 gas.[26] The 15 nm thick InAs membrane which is the top layer of the junction should prevent NO_2 from reaching the InAs/WSe_2 junction. After exposure to NO_2, the diode exhibited $\sim 10^3$ higher forward bias currents while maintaining an ideality factor of ~ 1.1 and a reverse bias current below the noise floor. In total, the diode exhibits a forward/reverse current ratio $>10^6$ for an applied voltage range of 2 V to -2 V. The slight gate dependence of the forward bias current indicates the change in the band-offset between the semiconductors by the gate potential.

In order to better understand the IV characteristics, electrostatic simulations were performed with TCAD Sentaurus

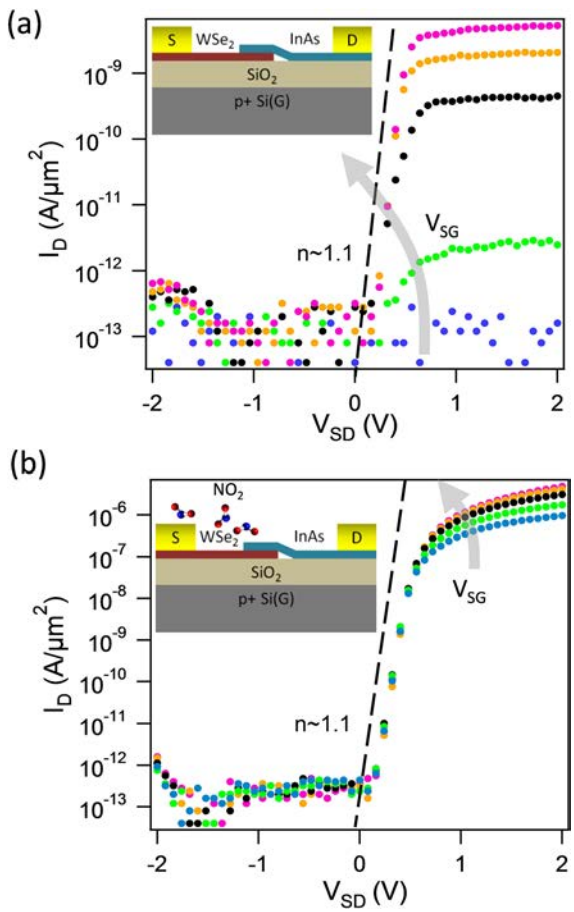

FIG. 2. I_D vs V_{SD} plots for an InAs/WSe_2 diode device with a [−4:2:4] V_{SG} bias (a) without NO_2 gas doping and (b) with NO_2 gas doping. The insets show the cross sectional schematics of the measured devices.

2012 to simulate the band structure of the InAs/WSe_2 diode with and without NO_2 doping. Hole and electron concentrations of $5 \times 10^{15}cm^{-3}$ and $1.5 \times 10^{18}cm^{-3}$ were used for WSe_2 and InAs, respectively, in the absence of NO_2 doping, as suggested by reports of their respective undoped thin films.[20,27] The WSe_2/Pd Schottky barrier height was determined by the difference between the semiconductor electron affinity and metal work function. The InAs/Pd Schottky barrier to the conduction band was assumed to be pinned at −0.15 eV as suggested by literature.[28] The simulation results without doping (Fig. 3(a)) suggest that the WSe_2/InAs p-n junction dominates the behavior at low forward biases, while a significant Schottky barrier to the WSe_2 valence band (i.e., a large parasitic resistance) will dominate at higher forward biases as observed experimentally. This is expected for any given diode in that the parasitic resistances lead to current saturation under large forward bias. From the band bending, we see that the majority of the depletion region lies in WSe_2. In order to simulate the band structure under NO_2 doping, a highly doped WSe_2 layer ($Na = 1 \times 10^{19}cm^{-3}$)[24] was introduced as shown in the inset of Figure 3(b). As discussed previously, it is assumed that the NO_2 has no effects on the InAs, InAs/Pd contact, and InAs/WSe_2 junction (since InAs is on top of WSe_2 and protects it from exposure to NO_2 in the junction area). The resulting band structure (Fig. 3(b)) shows dramatic thinning of the WSe_2 Schottky barrier, thus promoting hole tunneling through the barrier and reducing the WSe_2/Pd contact resistance. This finding is consistent with the experimental I-V curves (Fig. 2(b)), where the forward bias current

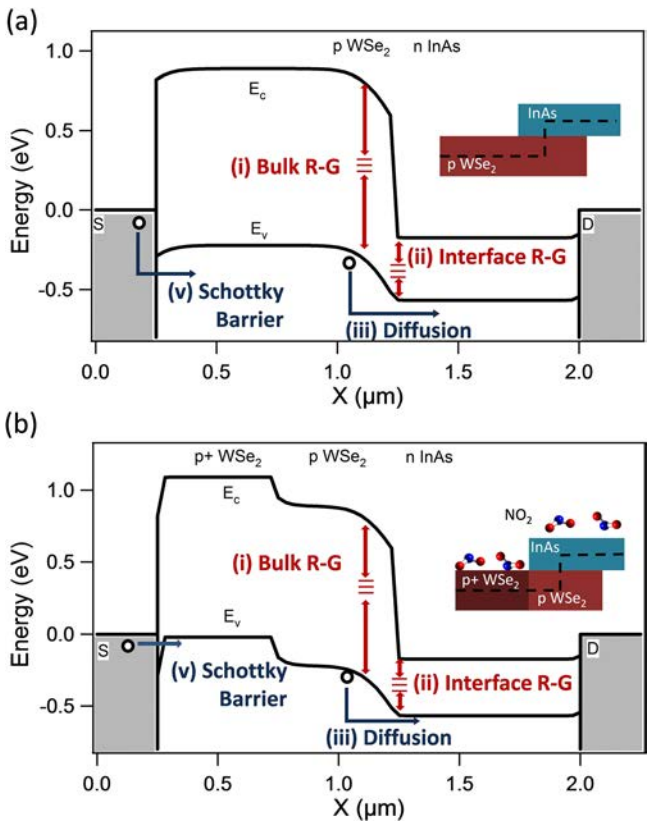

FIG. 3. Electrostatic band structure simulation results for an InAs/WSe_2 stack (a) without NO_2 gas doping and (b) with NO_2 gas doping. The insets show cross sectional schematics of the simulated structures. Important current processes are also shown.

is drastically enhanced by ~3 orders of magnitude upon NO_2 exposure.

In addition to a quantitative simulation of the diode band diagram, we analyze the heterodiode I-V characteristics to further understand the effect of each junction. Specifically, a standard diode's I-V characteristics can be described by five different regimes:[29] (i) reverse-bias, dominated by recombination-generation (R-G) current as well as drift current; (ii) low-voltage forward-bias, governed by R-G current; (iii) forward-bias, described by the ideal diode equations; (iv) high-injection forward-bias region, where diffusion current levels become so great that the injected minority carrier concentration equals the majority carrier concentration; and (v) series-resistance forward-bias region, where current is limited by parasitic resistances. The processes that drive these regimes in our device are depicted in Figure 3: specifically, R-G mechanisms (i, ii), diffusion over the p-n junction barrier (iii), and the parasitic resistance due to the Schottky barrier of the Pd/WSe_2 junction (v).

First, the reverse-bias current and low-voltage forward-bias current of the heterodiode will be considered. It should be noted that the measured current in reverse-bias is extremely low, below the 10^{-12} A/μm^2 noise floor of the measurement setup, and no R-G current dominated forward-bias regime is observed, suggesting that the RG current is nearly negligible in our devices. Such low RG current values can be ascribed to: first, the depletion region occurring entirely in the higher bandgap WSe_2 due to the higher carrier concentration in InAs; second, the small volume of the depletion region due to the relatively thin body of the WSe_2; and third, it is hypothesized that the density of interface traps existing at the InAs/WSe_2 interface must be low. Electron concentration levels previously extracted from similar InAs membranes without intentional doping[20] indicate that the InAs is doped high enough such that the depletion region is pushed mostly into the WSe_2, as shown in the band diagram simulations. Furthermore, WSe_2 Schottky FETs previously fabricated also show extremely low off currents, suggesting that WSe_2 R-G currents are below the noise floor of our measurements.[24] Next, we discuss the ideal diode region. This region is often described by the ideality factor, η, which ranges from $\eta = 1$ for an ideal diode to $\eta = 2$ for a R-G current dominated diode. Our device exhibits $\eta = 1.1$, further supporting the conclusion that the device has R-G current levels significantly lower than the diffusion current. Finally, the high forward bias region is dominated by the WSe_2/Pd Schottky barrier, which ultimately limits the forward-bias current. Note that the series resistance and high injection regimes cannot be clearly distinguished here given the relatively large resistance arising from the WSe_2/Pd Schottky contacts. In summary, our device exhibits an extremely low reverse bias RG current region, a nearly ideal diode region and a high forward bias region dominated by the WSe_2/Pd Schottky barrier, also supported by the experimental and simulation results in Figure 4. 2D simulations coupling Poisson's and drift diffusion relations were performed with TCAD Sentaurus 2012 to analyze the electrical characteristics of the heterostructure diode after NO_2 doping (Fig. 4). Ohmic contacts were assumed for the InAs/Pd and WSe_2/Pd junctions.[24,25] The forward current was fit with a series

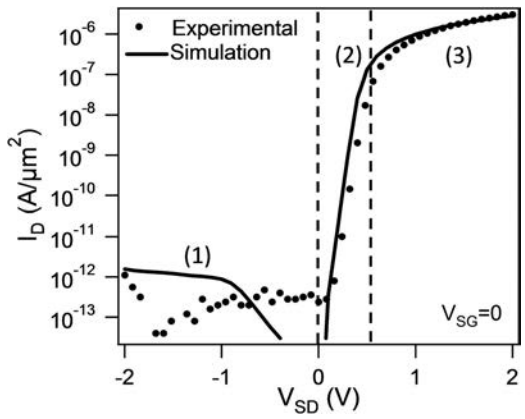

FIG. 4. Experimental and simulation results for an InAs/WSe_2 diode under NO_2 gas doping, depicting 3 areas of operation dominated by different processes: (1) recombination-generation, (2) ideal diode, and (3) parasitic resistances.

resistance of 5 kΩ/μm to account for parasitic resistances and the residual WSe_2/Pd Schottky barrier resistance, even after doping. The same doping concentrations mentioned in the previous paragraph were used. A low field minority carrier lifetime of 3×10^{-8}s and 10^{-9}s was assumed for InAs and WSe_2, respectively.[30,31] A uniform density of traps across the InAs bandgap at the InAs/WSe_2 interface with 10^{-15}cm^2 capture cross sections was assumed.[32] A density of interface traps of 10^{11} cm^{-2}eV^{-1} was used as a fitting parameter. The reasonable fit between simulation and experimental results indicates that the InAs/WSe_2 diode electrical behavior can be described well by standard diode theory.

In summary, a novel InAs/WSe_2 heterostructure, inconceivable by traditional epitaxial techniques alone, was fabricated by the layer transfer of each material. It exhibits an on/off current ratio $>10^6$ after reducing the WSe_2/Pd contact resistance with NO_2 doping, a clear indication of rectification from the InAs/WSe_2 junction. An ideality factor of ~1.1 was observed, indicating a clean interface between the two materials. Simulations of the observed IV characteristics indicate that its behavior can be explained by standard diode theory. This study paves way for the electrical analysis and understanding of a whole new avenue of heterojunctions previously thought impossible.

The materials preparation and characterization parts of this work were supported by the Director, Office of Science, Office of Basic Energy Sciences, and Division of Materials Sciences and Engineering of the U.S. Department of Energy under Contract No. De-Ac02-05Ch11231 and the Electronic Materials (E-Mat) program. Y.-L.C. acknowledges support from the National Science Council through Grant No. NSC 101-2112-M-007-015-MY3. The device characterization was supported by NSF Energy Efficient Electronics Science Center. A.J. acknowledges support from the World Class University program at Sunchon National University.

[1]H. Kroemer and J. Heber, Nature Mater. **9**, 372 (2010).
[2]L. Wang, E. Yu, Y. Taur, and P. Asbeck, IEEE Electron Device Lett. **31**, 431 (2010).
[3]R.-T. Huang, Y.-Y. Tu, D. Kasemset, N. Nouri, C. Colvard, and D. Ackley, J. Appl. Phys. **67**, 550 (1990).
[4]R. Dingle, H. L. Störmer, A. C. Gossard, and W. Wiegmann, Appl. Phys. Lett. **33**, 665 (1978).
[5]M. Wolf, Proc. IRE **48**, 1246 (1960).
[6]A. Koma, Thin Solid Films **216**, 72 (1992).
[7]K. Saikia, K. Uenoa, T. Shimadaa, and A. Koma, J. Cryst. Growth **95**, 603 (1989).
[8]M. P. Levendorf, C.-J. Kim, L. Brown, P. Y. Huang, R. W. Havener, D. A. Muller, and J. Park, Nature **488**, 627 (2012).
[9]L. Britnell, R. V. Gorbachev, R. Jalil, B. D. Belle, F. Schedin, A. Mishchenko, T. Georgiou, M. I. Katsnelson, L. Eaves, S. V. Morozov, N. M. R. Peres, J. Leist, A. K. Geim, K. S. Novoselov, and L. A. Ponomarenko, Science **335**, 947 (2012).
[10]W. J. Yu, Z. Li, H. Zhou, Y. Chen, Y. Wang, Y. Huang, and X. Duan, Nature Mater. **12**, 246 (2012).
[11]L. A. Ponomarenko, A. K. Geim, A. A. Zhukov, R. Jalil, S. V. Morozov, K. S. Novoselov, I. V. Grigorieva, E. H. Hill, V. V. Cheianov, V. I. Fal'ko, K. Watanabe, T. Taniguchi, and R. V. Gorbachev, Nat. Phys. **7**, 958 (2011).
[12]A. S. Mayorov, R. V. Gorbachev, S. V. Morozov, L. Britnell, R. Jalil, L. A. Ponomarenko, P. Blake, K. S. Novoselov, K. Watanabe, T. Taniguchi, and A. K. Geim, Nano Lett. **11**, 2396 (2011).
[13]C. R. Dean, A. F. Young, I. Meric, C. Lee, L. Wang, S. Sorgenfrei, K. Watanabe, T. Taniguchi, P. Kim, K. L. Shepard, and J. Hone, Nat. Nanotechnol. **5**, 722 (2010).
[14]T. Georgiou, R. Jalil, B. D. Belle, L. Britnell, R. V. Gorbachev, S. V. Morozov, Y.-J. Kim, A. Gholinia, S. J. Haigh, O. Makarovsky, L. Eaves, L. A. Ponomarenko, A. K. Geim, K. S. Novoselov, and A. Mishchenko, Nat. Nanotechnol. **8**, 100 (2013).
[15]H. Ko, K. Takei, R. Kapadia, S. Chuang, H. Fang, P. W. Leu, K. Ganapathi, E. Plis, H. S. Kim, S.-Y. Chen, M. Madsen, A. C. Ford, Y.-L. Chueh, S. Krishna, S. Salahuddin, and A. Javey, Nature **468**, 286 (2010).
[16]H. Fang, M. Madsen, C. Carraro, K. Takei, H. S. Kim, E. Plis, S.-Y. Chen, S. Krishna, Y.-L. Chueh, R. Maboudian, and A. Javey, Appl. Phys. Lett. **98**, 012111 (2011).
[17]A. C. Ford, C. W. Yeung, S. Chuang, H. S. Kim, E. Plis, S. Krishna, C. Hu, and A. Javey, Appl. Phys. Lett. **98**, 113105 (2011).
[18]M. Madsen, K. Takei, R. Kapadia, H. Fang, H. Ko, T. Takahashi, A. C. Ford, M. H. Lee, and A. Javey, Adv. Mater. **23**, 3115 (2011).
[19]K. Takei, S. Chuang, H. Fang, R. Kapadia, C.-H. Liu, J. Nah, H. S. Kim, E. Plis, S. Krishna, Y.-L. Chueh, and A. Javey, Appl. Phys. Lett. **99**, 103507 (2011).
[20]K. Takei, H. Fang, S. B. Kumar, R. Kapadia, Q. Gao, M. Madsen, H. S. Kim, C.-H. Liu, Y.-L. Chueh, E. Plis, S. Krishna, H. A. Bechtel, J. Guo, and A. Javey, Nano Lett. **11**, 5008 (2011).
[21]J. Nah, S. B. Kumar, H. Fang, Y.-Z. Chen, E. Plis, Y.-L. Chueh, S. Krishna, J. Guo, and A. Javey, J. Phys. Chem. C **116**, 9750 (2012).
[22]J. Nah, H. Fang, C. Wang, K. Takei, M. H. Lee, E. Plis, S. Krishna, and A. Javey, Nano Lett. **12**, 3592 (2012).
[23]C. Wang, J.-C. Chien, H. Fang, K. Takei, J. Nah, E. Plis, S. Krishna, A. M. Niknejad, and A. Javey, Nano Lett. **12**, 4140 (2012).
[24]H. Fang, S. Chuang, T. C. Chang, K. Takei, T. Takahashi, and A. Javey, Nano Lett. **12**, 3788 (2012).
[25]C. K. Peng, J. Chen, J. Chyi, and H. Morkoç, J. Appl. Phys. **64**, 429 (1988).
[26]P. Offermans, M. Crego-Calama, and S. H. Brongersma, Nano Lett. **10**, 2412 (2010).
[27]A. Jäger-Waldau and E. Bucher, Thin Solid Films **200**, 157 (1991).
[28]N. Li, E. S. Harmon, J. Hyland, D. B. Salzman, T. P. Ma, Y. Xuan, and P. D. Ye, Appl. Phys. Lett. **92**, 143507 (2008).
[29]S. M. Tze and K. K. Ng, *Physics of Semiconductor Devices*, 3rd ed. (John Wiley & Sons, New Jersey, 2007).
[30]A. Klein, Y. Tomm, R. Schlaf, C. Pettenkofer, W. Jaegermann, M. Lux-Steiner, and E. Bucher, Sol. Energy Mater. **51**, 181 (1998).
[31]V. Tetyorkin, A. Sukach, and A. Tkachuk, *Advances in Photodiodes* (InTech, 2011), p. 432.
[32]C. J. Park, H. B. Kim, Y. H. Lee, D. Y. Kim, T. W. Kang, C. Y. Hong, H. Y. Cho, and M. D. Kim, J. Cryst. Growth **227 228**, 1057 (2001).